Polypyrrole/Agarose-Based Electronically Conductive and Reversibly Restorable Hydrogel

Jaehyun Hur,[†] Kyuhyun Im,[‡] Sang Won Kim,[‡] Jineun Kim,[‡] Dae-Young Chung,[‡] Tae-Ho Kim,[‡] Kyoung Ho Jo,[§] Jong Hoon Hahn,[§] Zhenan Bao,[⊥] Sungwoo Hwang,[‡] and Nokyoung Park*[,‡]

[†]Department of Chemical and Biological Engineering, Gachon University, Seongnam, Gyeonggi 461-701, Republic of Korea, [‡]Frontier Research Laboratory, Samsung Advanced Institute of Technology, Samsung Electronics, Yongin, Gyeonggi 446-712, Republic of Korea, [§]Department of Chemistry, Pohang University of Science & Technology, Pohang 790-784, South Korea, and [⊥]Department of Chemical Engineering, Stanford University, Stanford, California 94305, United States

ABSTRACT Conductive hydrogels are a class of composite materials that consist of hydrated and conducting polymers. Due to the mechanical similarity to biointerfaces such as human skin, conductive hydrogels have been primarily utilized as bioelectrodes, specifically neuroprosthetic electrodes, in an attempt to replace metallic electrodes by enhancing the mechanical properties and long-term stability of the electrodes within living organisms. Here, we report a conductive, smart hydrogel, which is thermoplastic and self-healing owing to its unique properties of reversible liquefaction and gelation in response to thermal stimuli. In addition, we demonstrated that our conductive hydrogel could be utilized to fabricate bendable, stretchable, and patternable electrodes directly on human skin. The excellent mechanical and thermal properties of our hydrogel make it potentially useful in a variety of biomedical applications such as electronic skin.

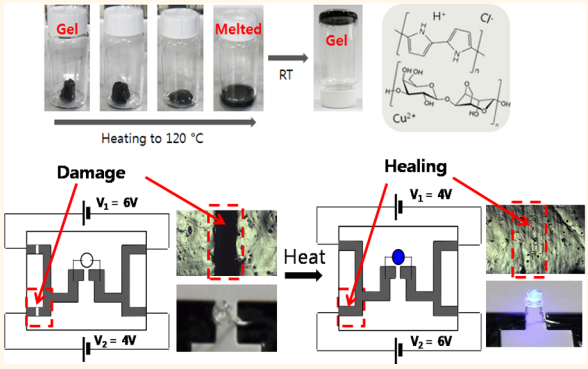

KEYWORDS: conductive hydrogel · agarose · polypyrrole · electrode · self-healing

Conductive hydrogels are polymeric composites that combine electrically conductive polymers with highly hydrated cross-linked hydrogels.[1,2] Due to excellent adhesion, porosity, and mechanical properties, conductive hydrogels are regarded as promising candidates for the fabrication of bioelectrodes, implantable biosensors, electro-stimulated drug release devices, and neural prostheses.[3−13] In particular, many conductive hydrogels are mechanically similar to human skin due to their high water content. As such, conductive hydrogels are promising materials for neutral interfaces in future devices, such as electronic skin (e-skin) and implantable microrobots.[12,14,15] In order to realize these promising applications, it is necessary to investigate fundamental properties of the gels before their usage can be extended to new research areas. For example, free shaping and patterning of the conductive target material is desired. In addition, if the material can be bent, stretched, and self-healed *via* external stimuli, it would be a truly "smart" material capable of the desired tasks. However, there are tremendous challenges in the practical execution of smart materials,[16−19] which explains why few reports address these issues and why most studies merely focus on the investigation of the two standard properties, namely, biocompatibility and conductivity.[3−13]

In this paper, we present a smart conductive hydrogel composite that possesses all essential properties including thermoplasticity and an ability to self-heal. Specifically, our conductive hydrogel is a network that maintains the properties of the original constituents and is synthesized by the kinetically controlled polymerization of monomers inside the thermoplastic hydrogel. By combining desirable properties of the conducting polymer and hydrogel, we demonstrate that our conductive hydrogel can be used to make reversibly self-healable and reshapable electrodes by thermal or spatially resolved, light-assisted healing.

* Address correspondence to n2010.park@samsung.com.

Received for review May 17, 2014 and accepted September 25, 2014.

Published online September 25, 2014
10.1021/nn502704g

In addition, we also demonstrate that bioelectrodes painted directly on biological surfaces are flexible, stretchable, and patternable. Such unique properties of our conductive smart hydrogel make it a promising material for future bioapplications.

RESULTS AND DISCUSSION

The conductive hydrogel is a binary composite material composed of polypyrrole and agarose (hereafter we call this APY gel), a linear polysaccharide derived from algae that allows the hydrogel to form reversibly in water depending on the temperature.[20−22] The rationale of employing the agarose instead of other types of hydrogels (*e.g.*, heparin gel, chitosan gel, alginate gel, *etc.*) is based on multiple aspects. The first reason is the thermal reversibility of agarose as a matrix. Most commercially available hydrogels (natural hydrogels such as heparin and alginate or synthetic hydrogels such as poly(vinyl alcohol)s and polyethylene glycols) cannot undergo reversible sol−gel transition due to their nature of chemical cross-linking. By contrast, the secondary hydrogen bonding (physical cross-linking) of agarose hydrogel (A-gel) makes it possible to experience the thermally reversible sol−gel transition.[23] The second reason is the thermodynamic property of an upper critical solution temperature (UCST) phase behavior of agarose. In the case of some reversible hydrogels such as chitosan[24] and poly(*N*-isopropylacrylamide),[25] despite their possible reversible sol−gel transition, their lower critical solution temperature phase behaviors are unable to be used as a template in our study because they are in the sol (liquid) state at room temperature. In that case, self-healing at room temperature cannot be realized. On the other hand, UCST phase behavior of agarose allows for the gel state at room temperature and sol (liquid) state at high temperature. Thus, these properties (physical cross-linking and UCST phase behavior) of agarose are best-suited for the framework of the hybrid gel in our study.

Polypyrrole (PPy) is one of the most widely used conducting polymers and is commonly prepared by the oxidative polymerization of pyrrole.[26−28] Among some oxidative agents, we used copper(II) chloride ($CuCl_2 \cdot 2H_2O$). The rationale for the choice of $CuCl_2$ as an oxidizing agent instead of commonly used ammonium persulfate (APS) and ferric chloride ($FeCl_3$) is based on the improved reversibility of the hybrid gel. When $FeCl_3$ was used as an oxidizing agent, it goes through the thermal reduction to form the Fe_2O_3 precipitate (hematite) at about 100 °C.[29,30] This temperature is close to the sol−gel transition of the agarose matrix. Therefore, Fe_2O_3 particles formed during the sol−gel transition of hybrid gel act as impurities and hinder the cross-linking of the hybrid gel, leading to the reduced number of thermal reversibility. Indeed, in our new experiment, we observed the solution color change from yellow (Fe^{3+} ion) to red (Fe_2O_3 particles) during the sol−gel transition of hybrid gel, indicating the formation of hematite. In using APS as an oxidizing agent, the increase of temperature up to ∼100 °C generates thermally dissociating radical initiators, and these highly reactive initiators prevent the reversible sol−gel transition of hybrid gel.[31,32]

In this study, we synthesized the conductive hydrogel by pyrrole polymerization inside the A-gel framework (Figure 1a). Since both pyrrole and PPy are immiscible with aqueous solvents,[33,34] the water-soluble oxidizing agent was mixed with melted A-gel at ∼40 °C and was then polymerized by adding pyrrole monomers to the mixture to improve the homogeneity of PPy distribution in the gel. As the temperature decreased to room temperature (∼25 °C), gelation of agarose and polymerization of pyrrole occurred simultaneously. During this process, most of the immiscible PPy and A-gel were mixed in the presence of an oxidizing agent as the mediator. The polymerization of pyrrole continued even after the gelation of agarose was complete, and PPy formed homogeneously along the three-dimensional network structure of A-gel. This polymerization process and the homogeneous formation of PPy can be easily confirmed by the color change from blue to black, as shown in Figure 1a. To better understand the polymerization process in the gel, we quantified the amount of PPy using thermogravimetric analysis (TGA) (Supporting Information Figure S1). It was found that for the different pyrrole concentrations ($c_{pyrrole}$ = 15, 75, and 450 mM), the weight fractions of PPy were calculated to be 3.8, 18.8, and 56.4%, respectively. The systematically increasing amount of PPy with increasing pyrrole concentration suggests the polymerization of pyrrole is not significantly hindered even inside the gel network. APY gel produced by this procedure underwent a reversible thermophase transition (Figure 1b), a characteristic property of A-gel, and showed a slightly different transition temperature with respect to the pyrrole concentration as measured by differential scanning calorimetry (Figure S2). The morphology of dried APY gel was observed using scanning electron microscopy (SEM) (Figures 1c−e). Compared with the A-gel, which has a smooth and thin multilayer structure, the APY gel displays rougher, thicker layers as the pyrrole concentration increases, which are an indication of the formation of PPy on the original A-gel (see atomic force microscopy images of APY gels at different pyrrole concentrations in Figures S3). To differentiate two different components clearly, the EDX mapping images for APY gel were taken as a function of pyrrole concentration ($c_{pyrrole}$ = 15, 50, and 150 mM). According to the images (Figure S4), the domain size of PPy (characterized by the nitrogen atom mapping images which are present only in PPy) systematically increases as the PPy concentration increases inside the hybrid

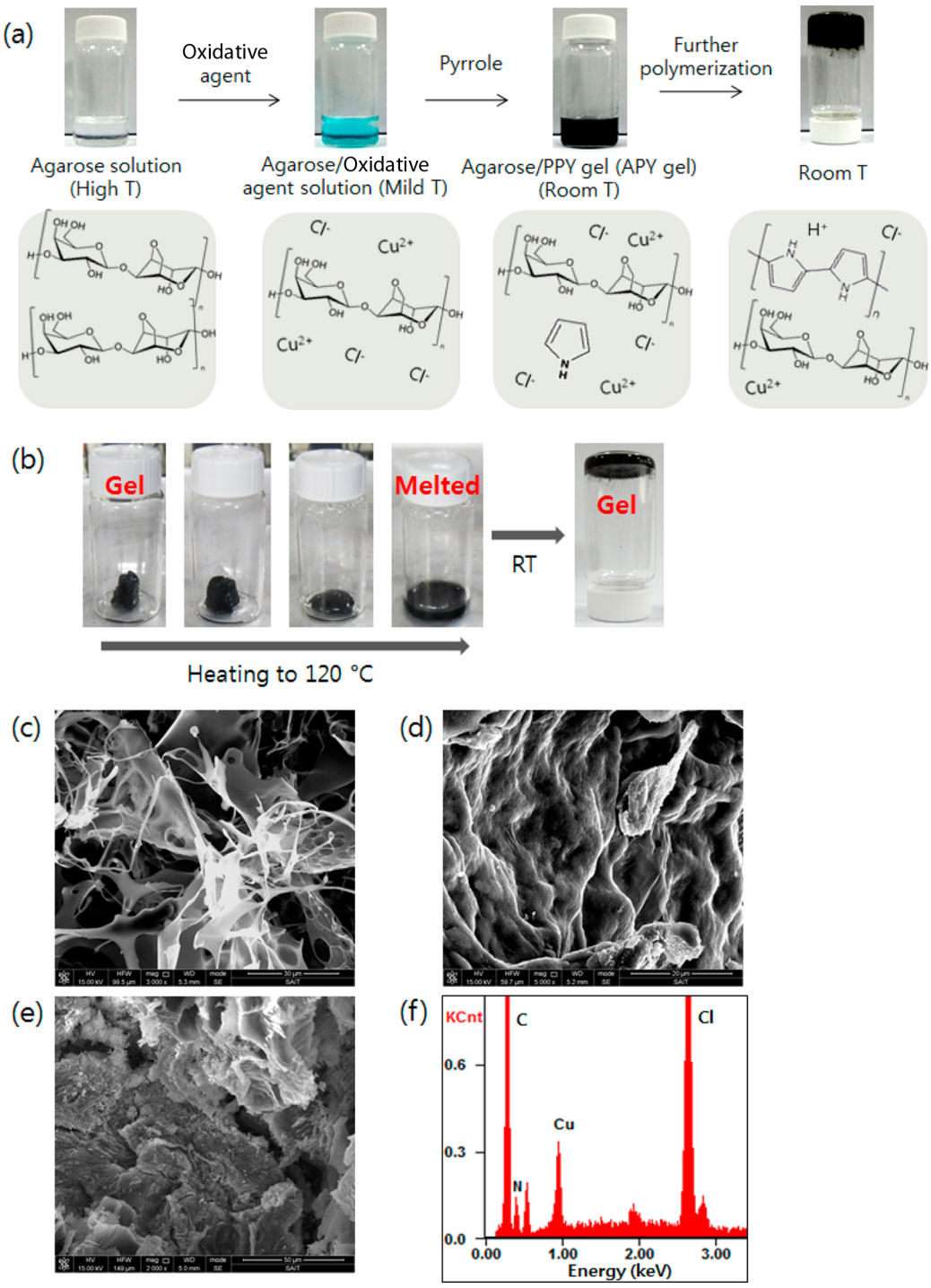

Figure 1. Synthetic route and morphology of the conductive hydrogel. (a) Schematic illustration of the synthetic procedure for the APY gel. (b) Photographic presentation of the thermoplastic reversibility (gel-melted-gel) of the APY gel. SEM images of APY gel at (c) $c_{pyrrole}$ = 0 mM, (d) $c_{pyrrole}$ = 30 mM, (e) $c_{pyrrole}$ = 150 mM, and (f) EDX analysis at $c_{pyrrole}$ = 30 mM.

gel. Additionally, Raman spectrum analysis of A-gel, PPy, and APY gel confirmed the presence of PPy on A-gel without altering the characteristic optical properties of A-gel or PPy during the APY gel formation (Figure S5).

Measurements of electrical, mechanical, and rheological properties were performed to further characterize APY gel. Hereafter, APY gel used for every experiment was in the hydrated state. The electrical conductivity was measured using a four-point probe method (measuring the surface conductivity), which gave results consistent with those measured by a conductivity meter (measuring the bulk conductivity) (Table S1). The electrical conductivity of the APY gel was found to be highly dependent on both the pyrrole concentration and the type of solvent used in the

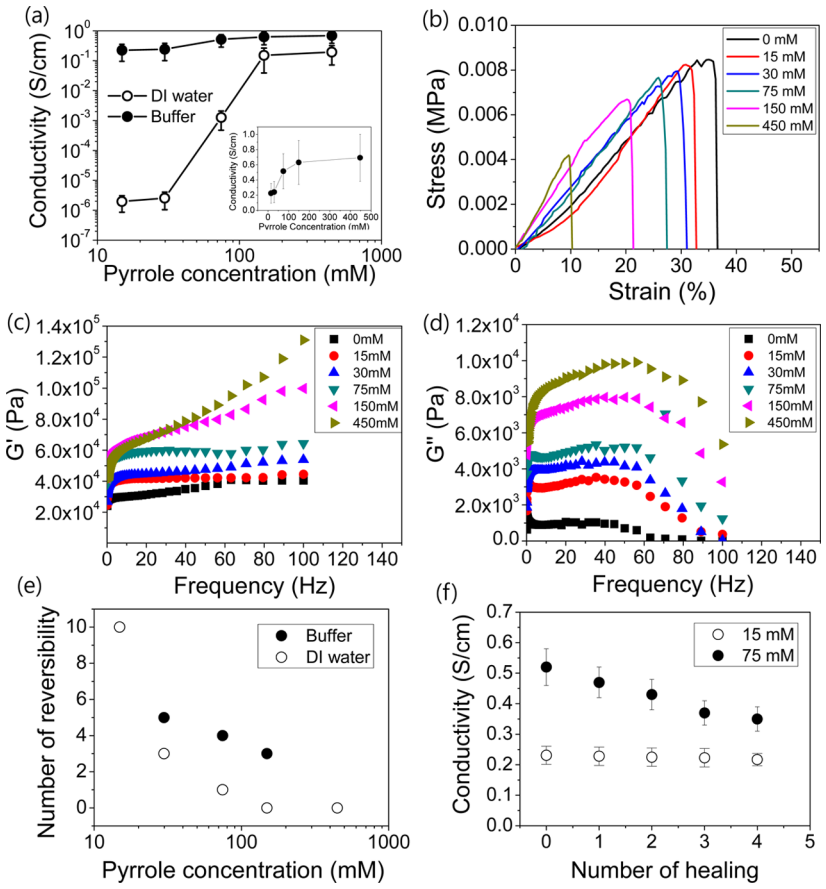

Figure 2. Electrical and viscoelastic properties of the APY gel. (a) Conductivity as a function of pyrrole concentration, (b) strain−stress curve, (c) storage modulus (G'), (d) loss modulus (G''), and (e) reversibility as a function of pyrrole concentration. For (a) and (e), measurements were performed for both DI-water-based and buffer-based APY gels. (g) Conductivity change as a function of repeated healing cycles at $c_{pyrrole}$ = 15 and 75 mM for buffer-based APY gel. Swelling ratios were 39.3, 32.0, 20.8, 13.3, and 5.9 for $c_{pyrrole}$ = 15, 30, 75, 150, and 450 mM, respectively.

experiments. When deionized (DI) water was used as the solvent for the APY gel, its electrical conductivity varied from 1.91×10^{-6} to 1.95×10^{-1} S/cm with increasing pyrrole concentration (Figure 2a) and reached a saturated value ($\sim 1.95 \times 10^{-1}$ S/cm) at a pyrrole concentration of 450 mM. When an ion-rich buffer solution (10× PBS) was used as a solvent for the APY gel, the conductivity was dramatically increased as a result of additional ionic currents induced by various ionic species present in the buffer medium (Figure 2a). Specifically, the increase in the conductivity was more significant with a lower concentration of pyrrole (less than 75 mM) as compared to that in DI water as a medium. Since APY gel is completely thermoreversible within a certain range of pyrrole concentrations (Figure 2f), the improvement of conductivity at a low pyrrole concentration range plays an important role in qualifying the APY gel as a highly conductive reversible hydrogel. For buffer-based APY gel, the increase of conductivity was further amplified by the addition of pyrrole due to the greater number of connected domains of PPy in the gel. The conductivity was increased from ~0.2 to ~0.7 S/cm as the pyrrole concentration increased from 15 to 450 mM, which is a 3.5-fold increase (inset of Figure 2a). The swelling ratios (the weight of fully swollen hydrogel to the weight of dried hydrogel) of gel were 39.3, 32.0, 20.8, 13.3, and 5.9 for $c_{pyrrole}$ = 15, 30, 75, 150, and 450 mM, respectively. The mechanical and viscoelastic properties of APY gel were measured by a uniaxial tensile test (UTT) and rotational rheometry (Figure 2b−d). It was found that the Young's modulus of APY gel increased from 28 ± 3 to 46 ± 64 kPa as the pyrrole concentration increased from 15 to 450 mM. The decreased strain at the breakage point of the APY gel fabricated with a higher pyrrole concentration is attributed to the high content of PPy, which is relatively rigid. For instance, while A-gel was stretched to about 35% of its original length at a given geometry (10 mm length × 3 mm width × 1 mm height), the APY gel with the highest pyrrole concentration (450 mM) was fractured at only 10% of its longitudinal stretching ratio. These results can be reasonably explained due to the deteriorated elasticity of the original A-gel brought on by the higher content of rigid PPY. This is consistent with previously reported results from the studies of composites consisting of elastic and rigid materials.[35,36] The frequency dependency of the oscillatory shear storage (G') and

loss (G'') moduli showed systematic behavior of the APY gel as a function of pyrrole concentration. Both the storage and loss moduli demonstrate a positive correlation with the pyrrole concentration, which is consistent with the results from the UTT. Although APY gel deviated from the state of original A-gel as the pyrrole concentration increased (G'' is positively related to the pyrrole concentration), the tendency of G' and G'' as a function of oscillation frequency was found to be similar to the original A-gel except at extremely high pyrrole concentrations (>150 mM). These results suggest that the APY gel retains the rheological properties of A-gel to the maximum extent when the PPy is formed along the A-gel network.

The viscoelastic properties as a function of surrounding temperatures were further investigated by observing the thermoplastic behavior of the APY gel (Figure 2e,f). Figure 2e presents the number of reversible phase transitions as a function of pyrrole concentration for DI-water-based and buffer-based APY gel. For the DI-water-based APY gel, a completely thermoreversible behavior can be seen when the pyrrole concentration is below 15 mM. As the pyrrole concentration increased, the reversibility of the APY gel decreased. This may be attributed to the breakage of a hydrogen bond by the acidic byproducts (HCl) generated during the polymerization of pyrrole ($C_4H_5N + CuCl_2 \rightarrow C_4H_4NCl + CuCl + HCl$).[26−28] Although the APY gel was carefully washed with DI water after gelation, HCl trapped inside the gel could not be completely removed. In fact, it rearranged itself in the APY gel matrix with multiple sol−gel transitions *via* diffusion, resulting in a reduced cross-linking density of APY gel. As confirmed by experiments conducted separately, the gelation of APY gel was sensitive to external stimuli such as the pH of the medium (Table S2). Thus, when the pyrrole concentration was extremely high (>450 mM), gelation would not initiate. Interestingly, for buffer-based APY gel, the thermoreversibility was significantly improved (Figure 2e), possibly because the PBS buffer solution moderated dramatic pH changes of the APY gel during the polymerization process and reduced the number of hydrogen bonds that were broken in the APY gel. As a result, the use of PBS buffer solution as a solvent for APY gel not only enhanced the gel conductivity by inducing additional ionic current but also broadened the viable pyrrole concentration range for APY demonstrating thermoplastic behavior. In general, it has been well-known that the conductivity of PPy increases as pH decreases due to the proton ion doping which causes the stabilization of charge carriers (polarons or bipolarons).[37] However, even with the buffer as a medium, lowering pH was limited in increasing the conductivity because the gelation did not even occur at too low pH (<5.3). Also, even for the hybrid gel ($c_{pyrrole}$ = 150 mM) immersed in different pH conditions (3.0, 4.5, 5.3, and 7.2) for ion doping, although the conductivity slightly increased (0.665, 0.654, 0.641, 0.631 S/cm, respectively), the reversibility of the gel was significantly deteriorated (the gel with pH lower than 5.3 did not show thermal reversibility any more). Figure 2f shows a plot of the conductivity variations as a function of the number of heat-induced phase (sol−gel) transitions at two different pyrrole concentrations for buffer-based APY gels. In both cases, the conductivity of APY gel demonstrated a negative linear relationship with the number of heat-induced phase transitions. This effect seems to be associated with reduced PPy percolation within the A-gel for repeated phase transitions and is caused by the phase separation between the water-immiscible PPy and aqueous A-gel. The conductivity decrease is more dominant for APY gels with higher pyrrole concentrations as more PPy percolations are disrupted by the repeated processes. For example, in the case of a high pyrrole concentration ($c_{pyrrole}$ = 75 mM), the conductivity decreased by ~33% after the phase transition was repeated four times, whereas the conductivity only decreased by ~6% for a low pyrrole concentration ($c_{pyrrole}$ = 15 mM) with the same number of transition processes (Figure 2f). This result suggests that the reversibility and conductivity recovery of our APY gel depend on both the APY gel medium and the pyrrole concentration in the initial synthesis. The conductivity of APY gel is also influenced by the temperature because the internal microscopic hybrid structure is changed as the temperature approaches the sol−gel transition temperature. This also gives the indirect picture of an internal percolation network variation as the temperature changes. For the APY gel at $c_{pyrrole}$ = 150 mM with buffer, the conductivities at 60, 80, 90, and 100 °C were measured to be 0.631, 0.628, 0.572, and 0.423 S/cm. This decrease of conductivity with increasing temperature, particularly close to sol−gel transition temperature, reflects the reduced number of PPy percolation networks as the hybrid gel undergoes the melting process. Conversely, this measurement gives insight that the gelation process of agarose induces the proper percolation network structure of PPy which contributes the the conductivity increase.

Although the characteristic elastic mechanical properties of conductive hydrogels are outstanding, potential applications of hydrogels in bendable or stretchable electrodes have rarely been reported. Here, to verify our APY gel as a suitable material for flexible electrodes, we have carried out systematic studies measuring the resistance variation of APY gel upon bending or stretching within the appropriate pyrrole concentration range. Figure 3a displays the resistance change as a function of bending angle for an APY gel slab (20 mm length × 5 mm width × 1 mm height, $c_{pyrrole}$ = 150 mM). It was found that, with a bending angle increase from 0 to 75°, the resistance increased

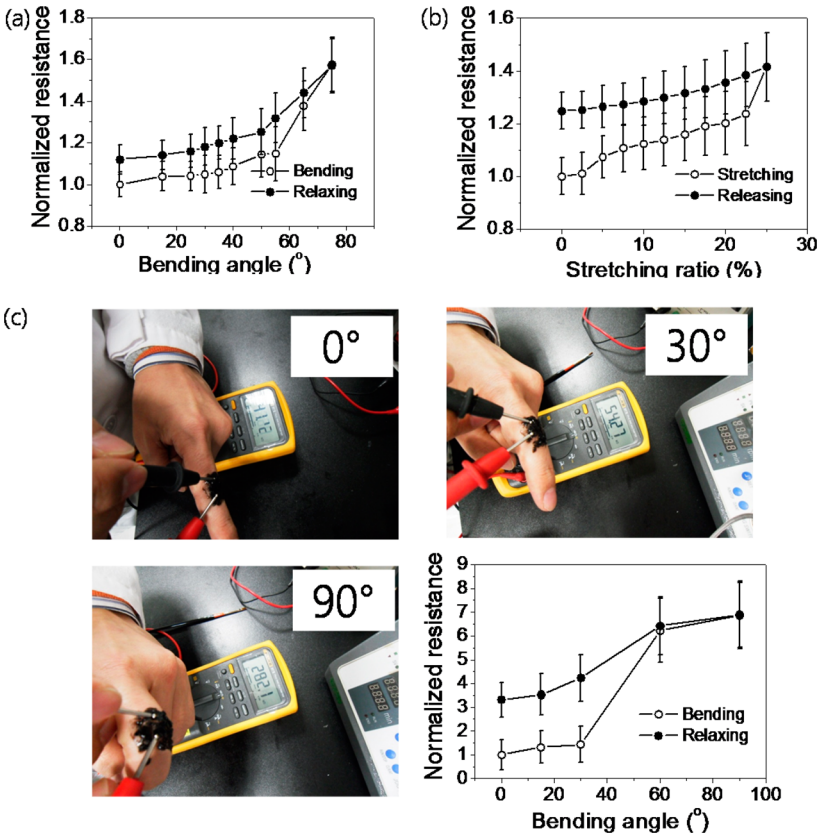

Figure 3. Bending and stretching resistance of the APY gel at $c_{pyrrole}$ = 150 mM. Variation of normalized resistances as functions of (a) bending angle (open circle, bending; closed circle, relaxing), (b) stretching ratio (open circle, stretching; closed circle, releasing). (c) Photographs of APY gel painted on a finger at different bending angles and resistance measured during the bending and relaxing process of the APY gel.

up to 158% of its original value (Figure 3a and Figure S6), most likely due to the breakage of PPy percolation inside the APY gel. Additionally, the resistance was measured as a function of film thickness with a bending test. As shown in Figure S7, the resistance increase as a function of bending angle was more pronounced as the thickness of the hybrid gel increased. For example, while there was merely 12% of normalized resistance increase at a bending angle of 65° for a thickness of 0.5 mm, it was as much as 61% for the thickness of 2.0 mm at the same conditions. In addition, the hysteresis of bending resistance was amplified as the thickness increased. The increase of normalized bending resistance after a cycle of bending was measured to be 2.5, 12.0, and 18.9% for the thicknesses of 0.5, 1.0, and 2.0 mm, respectively. On the other hand, resistance almost linearly increased with the increase of the stretching ratio in the stretching test (Figure 3b), where the APY gel slab sustained up to ~25% stretching along its longitudinal direction and gained ~40% more resistance (Figure S8). In both the bending and stretching tests, the resistance of the APY gel slightly increased (12 and 25% in bending and stretching tests, respectively) after one round of the deformation test. This hysteresis is caused by the rearrangement of PPy in the APY gel matrix and prevents the gel from returning to its original steady state. Furthermore, the APY gel can be painted on biological surfaces because the high viscosity of the melted APY gel facilitates adhesion to various biosurfaces such as human skin. This experiment was carried out by using a paint brush to paint APY gel in the melt state directly on the second joint of a forefinger of a demonstrator (Figure 3c) and monitoring the gel (after gelation) resistance variation as the finger was subjected to a bending−relaxing movement pattern. Although an increased relative resistance was found in this experiment compared to its resistance in the resting status, the bending resistance followed a similar variation (the resistance has been increased with increasing bending angle, and there was a hysteresis of resistance as a function of bending angle) as that in the slab measurement (graph in Figure 3c).

The ability of a gel electrode to be patterned into diverse shapes at different length scales is of vital importance, especially for applications in miniaturized sensors, microfluidic devices, biochips, and microdevices inside living organisms. Using the unique thermal properties of the APY gel electrode, the desired APY gel patterns could be fabricated with a broad range of patterning methods. Figure 4a illustrates an example of an APY gel electrode pattern transferred from a PDMS

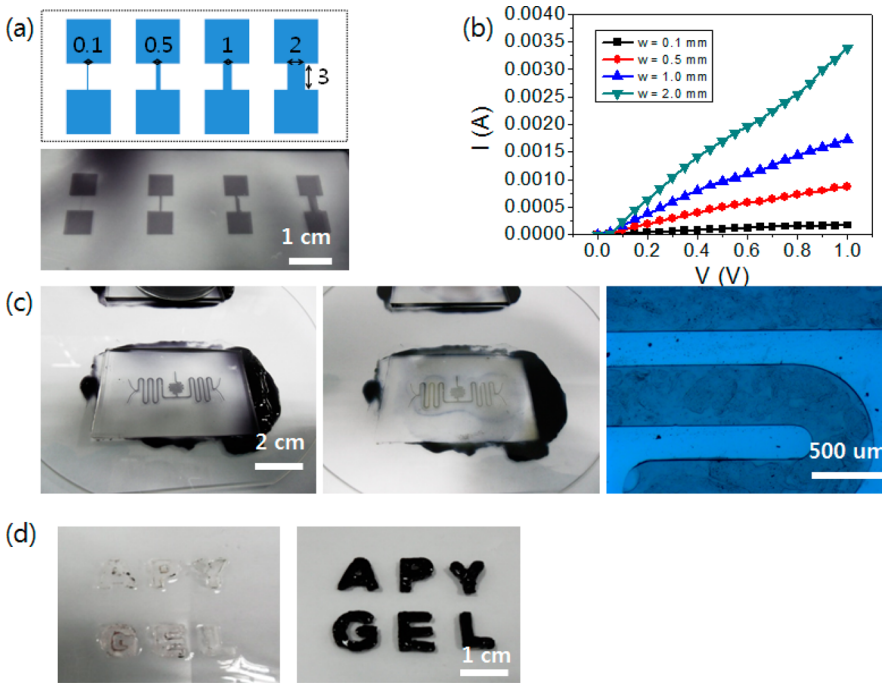

Figure 4. Patterning of the APY gel ($c_{pyrrole}$ = 150 mM) using a PDMS mold. (a) Square APY gel electrode arrays connected with gel wires (0.1, 0.5, 1.0, and 2.0 mm). (b) *I*–*V* measurement of square APY gel electrodes with different channel widths. (c) APY gel microcircuit electrode pattern transferred on glass. (d) Freestanding APY gel patterns.

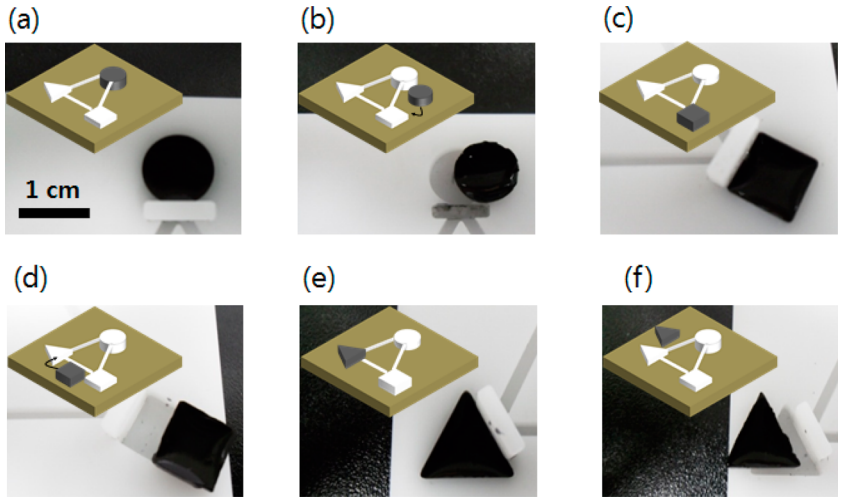

Figure 5. Thermoplasticity of the APY gel at $c_{pyrrole}$ = 75 mM. Schematic presentation and photographs of APY gel transformation in Teflon molds. (a) Molding a circular APY gel. (b) Circular APY gel detached from the mold. (c) Shaping a square APY gel by placing the circular gel into a square mold followed by heating and cooling. (d) Square APY gel detached from the mold. (e) Forming a triangular APY gel by repeating the reshaping process. (f) Triangular APY gel. The conductivity was slightly decreased throughout the transformation processes: 0.53 (circle), 0.48 (square), and 0.41 (triangle).

mold to a glass substrate ($c_{pyrrole}$ = 150 mM). The key strategies to obtain a complete transformation and intact APY gel pattern include a carefully controlled gel drying time, PDMS peeling speed, and UV-ozone treatment time. Square APY gel electrodes connected with diverse gel wires (0.1, 0.5, 1.0, and 2.0 mm width, 3.0 mm length, 100 μm height) were patterned (Figures 4), and as expected, the electrical resistance calculated from the *I*–*V* measurement systematically decreased with increasing wire width (Figure 4b). Due to the thermoplastic property, the formation of APY gel into diverse shapes (circle, square, and triangle) with different geometrical and dimensional attributes could be realized by utilizing a proper mold and by following a series of steps (Figure 5). To start the process, melted APY gel (80 °C, $c_{pyrrole}$ = 75 mM) was placed into a circular Teflon mold, which determines the circular shape of the gel, and cooled to room temperature (Figure 5a). Transformation of the circular APY gel into a square shape was carried out by transferring the

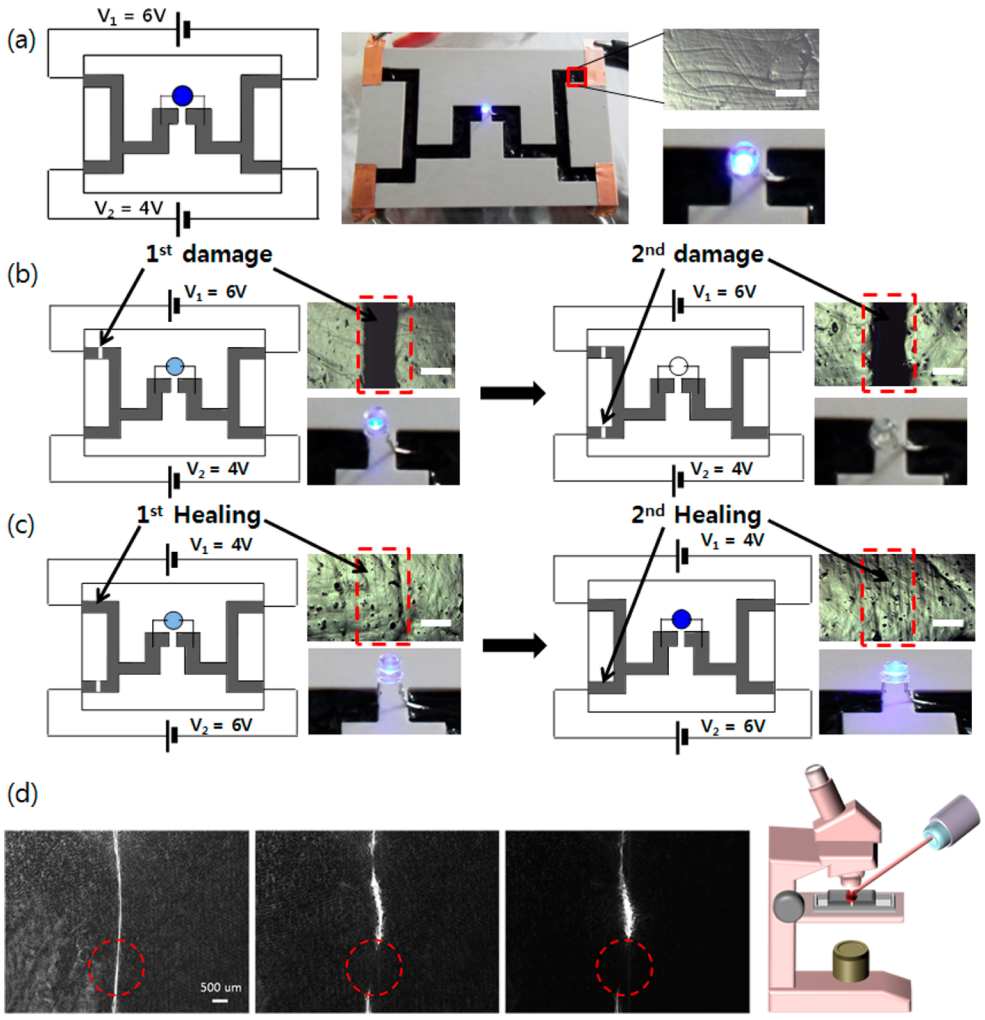

Figure 6. Thermal and optical healing of the APY gel at $c_{pyrrole}$ = 150 mM. (a) Cartoon and photograph of APY gel wire electric circuit for LED lighting. (b) First (arrow in the left panel) and second damage (arrow in the right panel) of APY gel in the electric circuit. Razor blade was used to create ~350 μm gaps in the APY gel. First damage reduced the brightness of the LED due to the open upper circuit (V_1 = 6 V and V_2 = 4 V), and second damage completely opened the circuit, resulting in the complete turn off of the LED light. (c) First (arrow in the left panel) and second healing (arrow in the right panel) of APY gel in the electric circuit. First healing (upper circuit) lighted the LED (V_1 = 4 V) and second healing (lower circuit) increased the brightness of the LED (V_2 = 6 V). The scale bars in (a–c) represent 350 μm. (d) Progress of local healing of APY gel indicated by the optical microscopic images by the cw laser diode at 644 nm.

circular APY gel into a square-shaped mold and heating until the gel melted. Upon cooling, the gel solidified into a gel state (Figure 5b,c). A series of melting–gelation–mold transfer steps can be carried out so that the same gel can be reused and reshaped multiple times by using appropriate templates as per requirements (Figure 5d–f). The electrical characterization for the shape-transformable gel was performed. Although the measured conductivity was slightly decreased as the melt/gelation process was repeated (0.53 (circle), 0.48 (square), and 0.41 S/cm (triangle)), the nature of the conductive hydrogel was maintained throughout the multiple transformation processes. The unique thermoplasticity of the gel is believed to contribute to this versatility.

The thermoplasticity of APY gel also makes it an attractive material for self-healing electrodes, which can self-repair damage in response to contact heating or noncontact optical stimuli. Figure 6a–c presents the sequential thermal damage-healing process of APY gel ($c_{pyrrole}$ = 150 mM) demonstrated with a LED light source powered by APY gel wires. First, the LED light was powered by two different voltages (V_1 = 6 V and V_2 = 4 V) *via* power suppliers connected in parallel (Figure 6a). The upper circuit was disconnected by cleaving the APY gel wire with a razor blade, and the LED light was dimmed as a result of the open upper circuit (left panel in Figure 6b). The subsequent disconnection of the second wire turned off the LED light completely (right panel in Figure 6b). The self-healing test was carried out by heating the circuit system directly on a hot plate. When the upper circuit was heated on the hot plate at 120 °C for ~30 min, the first damage induced by the wire scission was healed by following the melting–flowing–fusing process, and consequently, the LED activity was regained (left panel

in Figure 6c; now V_1 = 4 V and V_2 = 6 V). The relatively long heating time required to melt the APY gel wire was due to the thickness (6 mm) and poor thermal conductivity of the Teflon substrate. In the subsequent step, heating the entire circuit system (by placing the whole Teflon substrate on hot plate) resulted in a notable increase in LED brightness when higher voltage (V_2 = 6 V) was applied, suggesting the self-healing of the second damage (see right panel in Figure 6c). The APY gel wires were further inspected by an optical microscope, and the thermal healing effect was confirmed by the identification of a regenerated wire fragment (red dotted squares in Figure 6c) bridging the initial ~350 μm gap (black stripes enclosed by the dotted line in Figure 6b).

Nevertheless, there are limitations associated with this self-healing approach in regard to practical applications in biological subjects. Since the thermal healing requires high temperatures (~120 °C) and direct contact with the external heating source to initiate the process, it may not be directly applicable to biological surfaces. Moreover, this self-healing effect was only validated in macroscopic dimensions thus far. For biomedical applications, especially for microsized bio-organisms, noncontact healing is preferable as compared to contact healing, which relies on external heat stimuli. To overcome this problem, we took advantage of the photothermal properties of PPy, namely, the strong near-infrared (NIR) absorption and ability to convert light into thermal energy.[38,39] Figure 6d demonstrates the remote optical healing of APY gel using a 644 nm laser light as a heating source for microscopic healing. As shown in Figure S9, APY gel generously absorbs the light from the visible to NIR range due to the optical properties of PPy present in the APY gel. Notably, as a piece of cleaved APY gel slab was exposed to a focused laser light (500 mW/cm^2), the small damaged region (gap of ~100 μm) in APY gel was partially melted by the local photothermal effect and was healed during the gelation process while the gel was held at room temperature (Figure 6d).

CONCLUSION

In this study, we developed a new class of moldable, stretchable, and self-healable conductive hydrogels (APY gel) by utilizing an oxidizing agent as a mediator to induce homogeneous polymerization of the pyrrole monomer inside the three-dimensional agarose hydrogel network. This newly developed synthetic route provided well-defined, conductive hydrogels with well-preserved thermoplastic and conductive properties dictated by the primary components of the gel. Thermoplasticity and electrical conductivity of APY gel were systematically studied as functions of the pyrrole concentration and type of solvent for the APY gel. Although the gel conductivity increased, its thermoreversibility deteriorated with increasing pyrrole concentration. In particular, the APY gel was able to retain decent thermoplasticity, with ~0.35 S/cm conductivity, at pyrrole concentrations up to 150 mM. This is comparable with that of typical lab-synthesized conducting polymers such as PEDOT:PSS.[40] Although the mechanical properties of APY gel revealed progressive change depending on pyrrole concentration, its mechanical properties marginally resemble human tissue. Specifically, the Young's modulus of APY gel (27−46 kPa) is close to that of human skin (~5 kPa).[41] This mechanical property allowed APY gel to be directly painted on human skin and to be used as bendable and stretchable bioelectrodes. Furthermore, by using appropriate molds, APY gel electrodes can be reversibly formed into various shapes, with different aspect ratios and line scales (down to 100 μm line width and height/width aspect ratio of 1.0). Additionally, by taking advantage of the prominent characteristic attributes of the APY gel, such as thermoplasticity and conductivity, self-healing could be achieved in this study *via* external heat and light stimuli. In conclusion, many properties of APY gel shown in this article may be potentially useful in self-healable smart electrodes.

METHODS

Preparation of the APY Gel. Typically, 2 wt % agarose (Biorad) was dissolved in DI water by heating with a hot plate at 120 °C until the agarose was completely dissolved. The solution was cooled to a temperature of ~40 °C, where the solution remained in the liquid state. An appropriate amount of copper(II) chloride ($CuCl_2 \cdot 2H_2O$, Aldrich) was used as an oxidizing agent and dissolved in agarose solution at 40 °C. Notably, dissolution conducted at high temperatures (>90 °C) led to the reduction of the oxidizing agent and consequently prevented the polymerization of pyrrole. Pyrrole (Aldrich) was purified by silica gel column chromatography immediately before use and was subsequently added to the solution of oxidizing agent in agarose at a fixed molar ratio with respect to the oxidizing agent (pyrrole/oxidizing agent = 1:2).[26−28,42] After the solution was agitated for 10 min, the mixture was allowed to cool to room temperature. As the temperature decreased, the viscosity of the mixture increased and the color gradually changed to black, which are indications of the completion of gelation and polymerization, respectively. Even after the completion of gelation, the polymerization of pyrrole continued within the gel, as indicated by the color change. Therefore, a sufficient amount of time (a couple of days to a week) was allowed for further polymerization. When the polymerization was completed, APY gel was carefully washed with fresh DI water at least three times to remove unreacted species and byproducts.

Tensile and Dynamic Stress Measurements. Tensile mechanical properties of APY gel were measured from the uniaxial tensile test (Lloyd Instruments). For this test, a dog-bone-shaped APY gel sample was prepared (3 mm width × 10 mm length × 1 mm height). All measurements were performed at the same strain rate of 2 mm/min. Viscoelastic properties of APY gel were

measured using a rotational rheometer (Anton Paar Ltd., PhysicaRheometers UDS200) with a frequency ranging from 0.1 to 100 Hz; the APY gel was loaded on a 25 mm plate with 0.5 mm gap at 20 °C.

Bending and Stretching Tests. For the measurement of bending and stretching resistance, a cuboid APY gel slab (5 mm width × 20 mm length × 1 mm height) was prepared and inserted into two stainless steel blocks. To prevent the sliding of APY gel during the measurement, the APY gel was firmly secured by tightening the screws. The resistance of bending or stretching tests was measured from the *I*−*V* curve using a Keithley 2400 SourceMeter connected to a computer.

Thermal and Optical Healing of the APY Gel. To demonstrate the thermal healing of APY gel, a simple electric circuit (channel width of 6 mm and depth of 4 mm) was designed and made by polyether ketone, where melted APY gel ($c_{pyrrole}$ = 30 mM) was injected into the prefabricated channel and cured at room temperature. The LED bulb was embedded in the APY gel circuit during the gelation. In order to induce mechanical damage, a razor blade was used to create a ∼350 μm gap in the upper and lower circuits of the APY wires. For the sequential thermal healing test of APY gel, only the region containing the damage incurred by the first cut was heated by directly placing the upper half of the circuit on the hot plate at 120 °C, followed by placement of the entire circuit on the hot plate to investigate the self-healing of the second damage in the lower circuit. For the local optical healing of the APY gel, the same sample was placed on a PDMS substrate and cleaved to induce damage. In the middle of the damaged region, a coherent cube laser with 644 nm illumination was focused by a lens of 5 cm focal length and was applied for local healing. During the exposure, the melting process of APY gel was monitored by an optical microscope (Olympus LX71) equipped with a CCD camera (Lumenera).

Conductivity Measurements. In order to measure the conductivity of the gel, a slab of APY (20 (*l*) × 5 (*w*) × 1 mm (*t*)) was prepared through casting from a mold. The conductivity (σ) was calculated by the results from the measurement of sheet resistance (R_s) and thickness (*t*) defined by the following equation:

$$\sigma = \frac{1}{R_s t} \quad (1)$$

The sheet resistance was measured using a four-point probe with a linear probe head (1.0 gap mm, JANDEL HM21, UK).

Characterization of the Morphologies by SEM. The morphologies of freeze-dried APY gel at various pyrrole concentrations were analyzed using a field-emission scanning electron microscope (Hitachi S-4700, operation voltage of 15 keV). Osmium was sputtered onto the APY gel as a conductive coating for imaging purposes.

Raman Scattering Spectra. Raman scattering spectra with a resolution of about 1 cm^{-1} were collected in a backscattering configuration at room temperature using a Renishaw inVia Raman microscope. The samples were illuminated by a 514 nm He−Ne laser (power 4 mW) on a Leica microscope with a 20× objective.

Conflict of Interest: The authors declare no competing financial interest.

Acknowledgment. This work was supported by the Gachon University Research Fund of 2014 (Grant No. GCU-2014-0123). The authors also thank U.J. Yang for assistance in SEM imaging.

Supporting Information Available: TGA and DSC analysis of APY gel; comparison of surface roughness between A-gel and APY gel with AFM; EDX mapping on APY gel; Raman spectroscopy of A-gel, PPy, and APY gel; measurement of electrical conductivity for APY gel from a four-point probe method and conductivity meter; effect of medium on the gelation of APY gel (test of acidic and basic media); bending resistance of APY gel (photographs of measurement); stretching resistance of APY gel (photographs of measurements); absorbance of APY gel. This material is available free of charge *via* the Internet at http://pubs.acs.org.

REFERENCES AND NOTES

1. Green, R. A.; Baek, S.; Poole-Warren, L. A.; Martens, P. J. Conducting polymer−hydrogels for medical electrode applications. *Sci. Technol. Adv. Mater.* **2010**, *11*, 014107.
2. Guiseppi-Elie, A. Electroconductive hydrogels: Synthesis, characterization and biomedical applications. *Biomaterials* **2010**, *31*, 2701–2716.
3. Abidian, M. R.; Martin, D. C. Multifunctional nanobiomaterials for neural interfaces. *Adv. Funct. Mater.* **2009**, *19*, 573–585.
4. Kim, D.-H.; Abidian, M.; Martin, D. C. Conducting polymers grown in hydrogel scaffolds coated on neural prosthetic devices. *J. Biomed. Mater. Res., Part A* **2004**, *71*, 577–585.
5. Barthus, R. C.; Lira, L. M.; de Torresi, S. I. C. Conducting polymer−hydrogel blends for electrochemically controlled drug release devices. *J. Braz. Chem. Soc.* **2008**, *19*, 630–636.
6. Lira, L. M.; de Torresi, S. I. C. Conducting polymer−hydrogel composites for electrochemical release devices: Synthesis and characterization ofsemi-interpenetrating polyaniline−polyacrylamide networks. *Electrochem. Commun.* **2005**, *7*, 717–723.
7. Justin, G.; Guiseppi-Elie, A. Electroconductive blends of poly(HEMA-*co*-PEGMA-*co*-HMMA-*co*-SPMA) and poly(Py-*co*-PyBA): *In vitro* biocompatibility. *J. Bioact. Compat. Polym.* **2010**, *25*, 121–140.
8. Small, C. J.; Too, C. O.; Wallace, G. G. Responsive conducting polymer−hydrogel composites. *Polym. Gels Networks* **1997**, *5*, 251–265.
9. Tomer, R.; Dimitrijevic, D.; Florence, A. T. Electrically controlled release of macromolecules from cross-linked hyaluronic acid hydrogels. *J. Controlled Release* **1995**, *33*, 405–413.
10. Brahim, S.; Narinesingh, D.; Guiseppi-Elie, A. Polypyrrole−hydrogel composites for the construction of clinically important biosensors. *Biosens. Bioelectron.* **2002**, *17*, 53–59.
11. Moschou, E. A.; Madou, M. J.; Bachas, L. G.; Daunert, S. Voltage-switchable artificial muscles actuating at near neutral pH. *Sens. Actuators, B* **2006**, *115*, 379–383.
12. Siddhantaa, S. K.; Gangopadhyay, R. Conducting polymer gel: formation of a novel semi-IPN from polyaniline and cross-linked poly(2-acrylamido-2-methyl propanesulphonicacid). *Polymer* **2005**, *46*, 2993–3000.
13. Murdan, S. Electro-responsive drug delivery from hydrogels. *J. Controlled Release* **2003**, *92*, 1–17.
14. Abrahama, S.; Brahima, S.; Ishiharad, K.; Guiseppi-Elie, A. Molecularly engineered p(HEMA)-based hydrogels for implant biochip biocompatibility. *Biomaterials* **2005**, *26*, 4767–4778.
15. Tang, Q.; Wu, J.; Sun, H.; Lin, J.; Fan, S.; Hu, D. Polyaniline/polyacrylamide conducting composite hydrogel with a porous structure. *Carbohydr. Polym.* **2008**, *74*, 215–219.
16. Stuart, M. A. C.; Huck, W. Y. S.; Genzer, J.; Müller, M.; Ober, C.; Stamm, M.; Sukhorukov, G. B.; Szleifer, I.; Tsukruk, V. V.; Urban, M.; Winnik, F.; Zauscher, S.; Luzinov, I.; Minko, S. Emerging applications of stimuli-responsive polymer materials. *Nat. Mater.* **2010**, *9*, 101–113.
17. Sun, T.; Qing, G. Biomimetic smart interface materials for biological applications. *Adv. Mater.* **2011**, *23*, H57–H77.
18. Xia, F.; Jiang, L. Bio-inspired, smart, multiscale interfacial materials. *Adv. Mater.* **2008**, *20*, 2842–2858.
19. White, S. R.; Sottos, N. R.; Geubelle, P. H.; Moore, J. S.; Kessler, M. R.; Sriram, S. R.; Brown, E. N.; Viswanathan, S. Autonomic healing of polymer composites. *Nature* **2001**, *409*, 794–797.
20. Luo, Y.; Shoichet, M. S. A photolabile hydrogel for guided three-dimensional cell growth and migration. *Nat. Mater.* **2004**, *3*, 249–253.
21. Lewitus, D. Y.; Landers, J.; Branch, J. R.; Smith, K. L.; Callegari, G.; Kohn, J.; Neimark, A. V. Biohybrid carbon nanotube/agarose fibers for neural tissue engineering. *Adv. Funct. Mater.* **2011**, *21*, 2624–2632.
22. Ng, K. W.; Wang, C. C.-B.; Mauck, R. L.; Kelly, T.-A. N.; Chahine, N. O.; K, D. C.; G, A. A.; Hung, C. T. A layered agarose approach to fabricate depth-dependent

inhomogeneity in chondrocyte-seeded constructs. *J. Orthop. Res.* **2005**, *23*, 134–141.
23. Medina-Esquivel, R.; Freile-Pelegrin, Y.; Quintana-Owen, P.; Yáñez-Limón, J. M.; Alvarado-Gil, J. J. Measurement of the sol−gel transition temperature in agar. *Int. J. Thermophys.* **2008**, *29*, 2036–2045.
24. Goycoolea, F. M.; Argüelles-Monal, W. M.; Lizardi, J.; Peniche, C.; Heras, A.; Galed, G.; Díaz, E. I. Temperature and pH-sensitive chitosan hydrogels: DSC, rheological and swelling evidence of a volume phase transition. *Polym. Bull.* **2007**, *58*, 225–234.
25. Li, C.; Alam, M. M.; Bolisetty, S.; Adamcik, J.; Mezzenga, R. New biocompatible thermo-reversible hydrogels from PNiPAM-decorated amyloid fibrils. *Chem. Commun.* **2011**, *47*, 2913–2915.
26. Zhang, X.; Bai, R. Surface electric properties of polypyrrole in aqueous solutions. *Langmuir* **2003**, *19*, 10703–10709.
27. Zhang, J.; She, Y.; Lu, B.; Zhou, Y.; Fu, K. A new method on the chemical synthesis of doped polypyrrole initiated by $CuCl_2-C_2H_5OH$ system. *Chin. J. Polym. Sci.* **1993**, *11*, 337–341.
28. Deronzier, A.; Moutet, J.-C. Polypyrrole films containing metal complexes: syntheses and applications. *Coord. Chem. Rev.* **1996**, *147*, 339–371.
29. Dutrizac, J. E.; Riveros, P. A. The precipitation of hematite from ferric chloride media at atmospheric pressure. *Metall. Mater. Trans. B* **1999**, *30B*, 993–1001.
30. Khoiroh, L. M.; Mardiana, D.; Sabarudin, A.; Ismuyanto, B. Synthesis of Hematite Pigments (α-Fe2O3) by Thermal Transformations of FeOOH. *J. Pure Appl. Chem. Res.* **2013**, *2*, 27–34.
31. Hosseinzadeh, H. Chemical modification of sodium hyaluronate *via* graft copolymerization of acrylic acid using ammonium persulfate. *Res. J. Pharm. Biol. Chem. Sci.* **2012**, *3*, 756–761.
32. Kohut-Svelko, N.; Pirri, R.; Asua, J. M.; Leiza, J. R. Redox initiator systems for emulsion polymerization of acrylates. *J. Polym. Sci. A: Polym. Chem.* **2009**, *47*, 2917–2926.
33. Park, S.; Kwon, T.-G.; Park, S.-I.; Kim, S.; Kwak, J.; Lee, S.-Y. Conductive microrod preparation by molecular self-assembly and polymerization. *RSC Adv.* **2013**, *3*, 8468–8473.
34. Omastová, M. R.; Trchová, M.; Kovářová, J.; Stejskal, J. Synthesis and structural study of polypyrroles prepared in the presence of surfactants. *Synth. Met.* **2003**, *138*, 447–455.
35. Pojanavaraphan, T.; Magaraphan, R. Fabrication and characterization of new semiconducting nanomaterials composed of natural layered silicates (Na^+-MMT), natural rubber (NR), and polypyrrole (PPy). *Polymer* **2010**, *51*, 1111–1123.
36. Velasco-Santos, C.; Martínez-Hernández, A. L.; Fisher, F. T.; Ruoff, R.; Castan, V. M. Improvement of thermal and mechanical properties of carbon nanotube composites through chemical functionalization. *Chem. Mater.* **2003**, *15*, 4470–4475.
37. Ansari, R. Polypyrrole conducting electroactive polymers: Synthesis and stability studies. *Electron. J. Chem.* **2006**, *3*, 186–201.
38. Yang, K.; Xu, H.; Cheng, L.; Sun, C.; Wang, J.; Liu, Z. *In vitro* and *in vivo* near-infrared photothermal therapy of cancer using polypyrrole organic nanoparticles. *Adv. Mater.* **2012**, *24*, 5586–5592.
39. Zha, Z.; Yue, X.; Ren, Q.; Dai, Z. Uniform polypyrrole nanoparticles with high photothermal conversion efficiency for photothermal ablation of cancer cells. *Adv. Mater.* **2013**, *25*, 777–782.
40. Ner, Y.; Invernale, M. A.; Grote, J. G.; Stuart, J. A.; Sotzing, G. A. Facile chemical synthesis of DNA-doped PEDOT. *Synth. Met.* **2009**, *160*, 351–353.
41. Daly, C. H. Biomechanical properties of dermis. *J. Invest. Dermatol.* **1982**, *79*, 17s–20s.
42. Brezoi, D.-V. Polypyrrole films prepared by chemical oxidation of pyrrole in aqueous $FeCl_3$ solution. *J. Sci. Arts* **2010**, *12*, 53–58.